Invisible RNA state dynamically couples distant motifs

Janghyun Lee[a], Elizabeth A. Dethoff[b], and Hashim M. Al-Hashimi[c,1]

[a]Department of Chemistry, University of Michigan, Ann Arbor, MI 48109-1055; [b]Department of Chemistry, University of North Carolina at Chapel Hill, Chapel Hill, NC 27599-3290; and [c]Department of Biochemistry and Chemistry, Duke University School of Medicine, Durham, NC 27710

Edited by Dinshaw J. Patel, Memorial Sloan–Kettering Cancer Center, New York, NY, and approved May 27, 2014 (received for review April 30, 2014)

Using on- and off-resonance carbon and nitrogen R1ρ NMR relaxation dispersion in concert with mutagenesis and NMR chemical shift fingerprinting, we show that the transactivation response element RNA from the HIV-1 exists in dynamic equilibrium with a transient state that has a lifetime of ∼2 ms and population of ∼0.4%, which simultaneously remodels the structure of a bulge, stem, and apical loop. This is accomplished by a global change in strand register, in which bulge residues pair up with residues in the upper stem, causing a reshuffling of base pairs that propagates to the tip of apical loop, resulting in the creation of three noncanonical base pairs. Our results show that transient states can remodel distant RNA motifs and possibly give rise to mechanisms for rapid long-range communication in RNA that can be harnessed in processes such as cooperative folding and ribonucleoprotein assembly.

NMR spectroscopy | dynamics | R1ρ relaxation dispersion | nucleic acids

It is now well-established that RNA sequences do not code for a single static structure, but rather, many conformations that populate energetic minima along a free-energy landscape (1, 2). Cellular inputs, ranging from changes in temperature and pH to the binding of proteins, other RNAs, and ligands, can preferentially stabilize select conformations along the landscape, resulting in dynamic changes in RNA structure that drive the multistep catalytic cycles of ribozymes (3), regulatory activities of riboswitches (4) and other RNA-based switches (5), and the dynamic assembly and disassembly of ribonucleoprotein (RNP) complexes (6).

A common mode of RNA dynamics involves rearrangements in secondary structure that can melt or create entire hairpins, and thereby expose or sequester key regulatory elements that are several nucleotides long (1, 4, 7, 8). Such secondary structural transitions entail large kinetic barriers, so they are often catalyzed by RNA-binding proteins (9), ATP-dependent chaperones (10), or otherwise occur by modulating cotranscriptional folding (5, 11). Recently, NMR R1ρ relaxation dispersion experiments (12–15) in concert with mutagenesis (16) have helped uncover more labile RNA secondary structural transitions that can take place without assistance from external cofactors at rates that are 2–4 orders of magnitude faster than larger-scale secondary structural rearrangements. These transitions entail excursions away from the energetically favorable ground state (GS) toward low-populated (typically populations <15%) and short-lived (lifetime < milliseconds) species often referred to as "excited states" (ES) (12, 13). These invisible RNA ES feature localized reshuffling of base pairing in and around noncanonical motifs such as bulges, internal loops, and apical loops (16) which can also expose or sequester functionally important residues or promote ATP-independent large-scale changes in secondary structure (14, 15). These faster and more localized changes in secondary structure may meet unique demands in RNA-based regulatory functions (16).

Using NMR carbon R1ρ relaxation dispersion (17–19), we recently reported (16) that the apical loop of the transactivation response element (TAR) from the HIV-1 RNA (20) rapidly exchanges ($k_{ex} = k_1 + k_{-1} = \sim 25$ kHz) with an ES that has a population (p_B) of ∼13% and exceptionally short lifetime (τ) of ∼45 μs (Fig. 1*A*). TAR is a regulatory viral RNA element located at the 5′ end of the HIV-1 retroviral genome that plays many roles in viral replication, including transcription elongation (21), translation (22), dimerization (23), packaging (23), and viral latency (24). TAR contains two functionally important motifs that are separated by four Watson–Crick base pairs: a trinucleotide bulge and a hexanucleotide apical loop (25, 26) (Fig. 1*A*). The TAR bulge and apical loop form two distinct flexible sites for binding a variety of proteins (27, 28) as well as small molecules that are being developed as anti-HIV therapeutics (29, 30). In the GS, apical loop residues C30, U31, G32, and A35 are exposed and available to interact with proteins (25, 26) (Fig. 1*A*). However, in the ES (which we will refer to as ES1), C30, U31, G34, and A35 are sequestered into noncanonical base pairs and therefore are less available for intermolecular interactions (16) (Fig. 1*A*). Indeed, mutations that stabilize ES1 are correlated with reductions in TAR-transactivator of transcription (Tat)-cyclin T1 binding affinities as well as reduced efficiencies in Tat-mediated transcriptional activation, possibly implying a functional role for ES1 (16).

During the course of our studies (16), we also observed that two apical loop residues, G33 and A35, uniquely sense a slow exchange process, whereas most other apical loop residues, including A35, sense fast exchange to ES1 (16). This slow exchange process is directed toward a second distinct ES (which we will refer to as ES2), which has a lower population ($p_B \sim 0.4\%$) and longer lifetime ($\tau \sim 2$ ms) compared with ES1. It is striking that whereas the sugar moiety of A35 (A35–C1′) senses fast exchange to ES1, the base moiety of the same residue (A35–C8) senses slow exchange to ES2 (16). The structure of ES2, and whether it involves localized conformational changes in G33 and A35, or a more extensive conformational rearrangement, remains unknown.

Here, we perform carbon as well as nitrogen R1ρ NMR relaxation dispersion experiments targeting a much broader set of residues in wild-type TAR, including the lower stem, bulge, and upper stem, aimed at characterizing ES2. To the best of our

Significance

We recently showed, using NMR relaxation dispersion, that the HIV-1 transactivation response element (TAR) RNA forms a transient state (lifetime ∼45 μs and population ∼13%) through localized changes in base pairing within the apical loop. Here, we report a second transient TAR state that has longer lifetime (∼2 ms) and smaller population (∼0.4%) that simultaneously remodels the bulge and apical loop, which are separated by four Watson–Crick base pairs. This is accomplished by a global change in the register of bulge residues, which pair up with residues in the upper stem, causing reshuffling of base pairs that propagates to the apical loop and creation of three noncanonical base pairs. Thus, transient states provide a mechanism for dynamically coupling distant RNA motifs.

Author contributions: J.L. and H.M.A.-H. designed research; J.L. and E.A.D. performed research; J.L. and H.M.A.-H. analyzed data; and J.L., E.A.D., and H.M.A.-H. wrote the paper.

The authors declare no conflict of interest.

This article is a PNAS Direct Submission.

[1]To whom correspondence should be addressed. E-mail: hashim.al.hashimi@duke.edu.

This article contains supporting information online at www.pnas.org/lookup/suppl/doi:10.1073/pnas.1407969111/-/DCSupplemental.

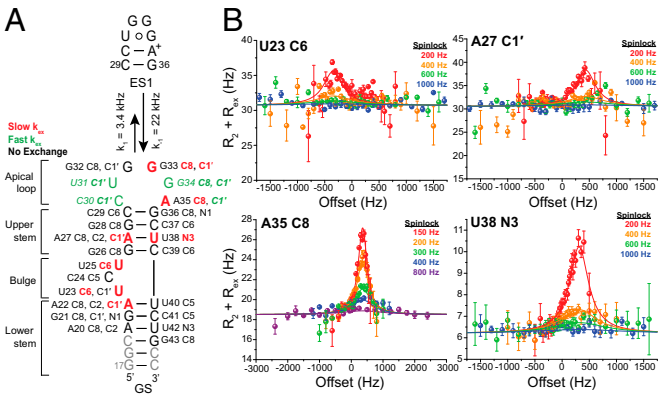

Fig. 1. Slow R1ρ relaxation dispersion in HIV-1 TAR. (*A*) Secondary structure of HIV-1 TAR GS showing exchange with ES1. Sites showing slow, fast, and no chemical exchange are highlighted in red, green, and black, respectively. Sites highlighted in gray were not measured due to spectral overlap. (*B*) Representative examples of on-resonance and off-resonance relaxation dispersion profiles showing dependence of $R_2 + R_{ex}$ on spinlock power and both spinlock power and offset. Shown are global fits (solid line) to a two-state model using the Laguerre equation (Eq. **S1**). Error bars represent experimental uncertainty (1 SD) as determined from propagation of errors obtained from monoexponential fitting of duplicate sets of R1ρ data and analysis of signal-to-noise.

knowledge, this is the first study reporting the measurement of ^{15}N relaxation dispersion data in RNA, thus extending prior studies on DNA (31). Our results uncover a dramatic ES2 structure that results in correlated changes in the bulge, upper stem, and apical loop through a long-range process involving the upward migration of two bulge residues across the upper stem and into the apical loop. Our results show that transient states can dynamically couple distant motifs and give rise to mechanisms for rapid and efficient long-range communication in RNA.

Results and Discussion

Characterization of Slow Exchange Involving the HIV-1 TAR Bulge and Apical Loop. To obtain further insights into ES2, we performed carbon as well as nitrogen R1ρ NMR relaxation dispersion experiments at 25 °C targeting sites throughout HIV-1 TAR. Interestingly, we observed significant carbon and nitrogen relaxation dispersion and evidence for slow exchange at several sites in the upper stem (A27–C1′ and U38–N3), bulge (U23–C6 and U25–C6), and even lower stem (A22–C1′) (Fig. 1 *A* and *B*). Several sites showed no signs of exchange, including A20, G21, U42, and G43 in the lower stem and G26, C29, G36, C37, and C39 in the upper stem (Fig. S1). A two-state analysis ($A \underset{k_B}{\overset{k_A}{\rightleftharpoons}} B$) of these R1ρ relaxation dispersion data (Fig. 1*B* and Fig. S2) using the Laguerre equation (32) yielded an ES population ($p_B \sim 0.26$–0.66%) and lifetime ($\tau = 1.2$–3.1 ms) very similar to that measured previously (16) for the slow-exchanging apical loop residues ($p_B = \sim 0.4\%$ and $\tau = \sim 2$ ms). Indeed, all of the R1ρ data showing signs of slow exchange could be combined into a single two-state global fit yielding $p_B = 0.40 \pm 0.05\%$ and $\tau = 2.1 \pm 0.3$ ms (Table S1).

The similar slow exchange parameters observed for sites in the apical loop, upper stem, bulge, and lower stem could potentially arise from a single transition toward an ES2 that simultaneously remodels the structures of the bulge, upper stem, and apical loop. To test this hypothesis, we examined the impact of omitting the bulge on relaxation dispersion measured in the apical loop (TAR-Δbulge, Fig. 2*A*). Omitting the bulge had little to no effect on the TAR GS chemical shifts, including those in the upper stem and apical loop (16). Likewise, omitting the bulge had no detectable effect on relaxation dispersion measured for fast-exchanging resonances in the apical loop (Fig. 2*A*). This is as expected given that ES1 involves the local reshuffling of base pairing within the apical loop itself (16) (Fig. 1*A*). In stark contrast, omitting the bulge completely quenched relaxation dispersion measured at slow-exchanging apical loop resonances G33–C8, G33–C1′, and A35–C8, which are four base pairs away from the deleted bulge (Fig. 2*A*). It is striking that omitting the bulge surgically quenches slow exchange at A35–C8 without affecting fast exchange at A35–C1′ in the same residue (Fig. 2*A*). These results demonstrate that slow exchange in the apical loop is strongly dependent upon the TAR bulge.

As an inverse experiment, we examined the consequence on relaxation dispersion measured in the TAR bulge when replacing the wild-type (WT) hexanucleotide apical loop with a more stable UUCG tetraloop (TAR-UUCG, Fig. 2*B*). Again, this replacement had little to no effect on the chemical shifts, including those measured in the lower stem and bulge (33). However, it completely quenched the newly measured relaxation dispersion at the bulge and upper stem (A22–C1′, U23–C6, A27–C1′, and U38–N3, Fig. 2*B*). These results demonstrate that slow exchange at the bulge is strongly dependent upon the WT TAR apical loop.

The absence of relaxation dispersion at U23–C6 in TAR-UUCG is inconsistent with a previous study (34) reporting significant relaxation dispersion at U23–C6 in TAR-UUCG using Carr–Purcell–Meiboom–Gill (CPMG) relaxation dispersion experiments and a TAR sample prepared using solid-phase

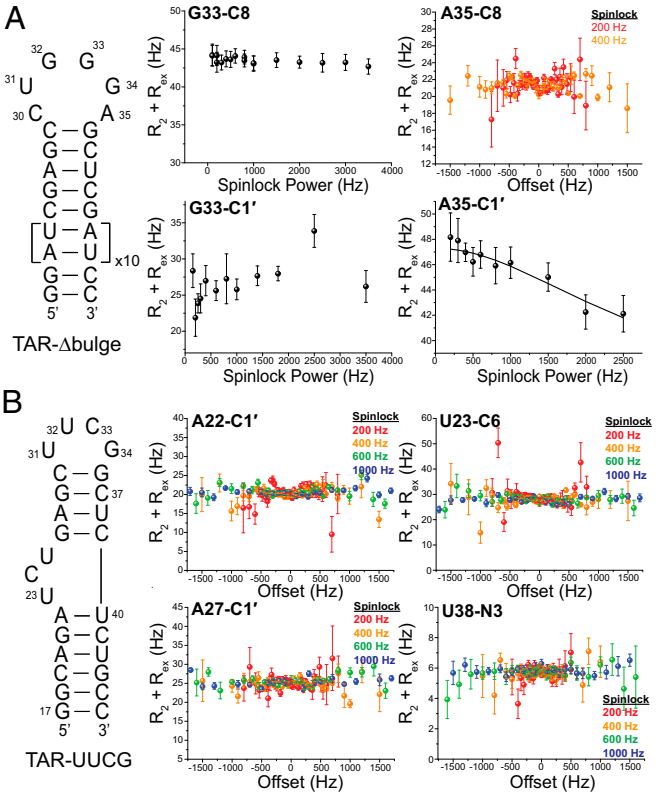

Fig. 2. Codependence of slow relaxation dispersion in the TAR bulge and apical loop. (*A*) Deleting the TAR bulge (TAR-Δbulge) selectively quenches slow exchange in the TAR apical loop without affecting fast exchange. (*B*) Replacement of the WT TAR apical loop with UUCG (TAR-UUCG) quenches slow relaxation dispersion in the bulge and the upper stem. Error bars in *A* and *B* represent experimental uncertainty (1 SD) as determined from propagation of errors obtained from monoexponential fitting of duplicate sets of R1ρ data and analysis of signal-to-noise.

synthesis containing ^{13}C6-enriched pyrimidines. The exchange parameters obtained for U23–C6 in TAR-UUCG in the previous study (34) are within error with those obtained here at 25 °C for TAR containing the WT apical loop (Table S1). We did not observe relaxation dispersion for U23–C6 in TAR-UUCG when using the same buffer conditions as those used in the CPMG study (34) (Fig. S3). These differences could arise from differences in sample preparation and/or experiments used to measure relaxation dispersion.

Characterizing the Structure of ES2 Using Structure Prediction and Chemical Shifts. The two-state analysis of the resonance relaxation dispersion data also yields the ES2 carbon and nitrogen chemical shifts which carry important information about the ES2 structure, including the orientation of bases (*syn* versus *anti*), sugar pucker, and stacking (Table S1). The significantly upfield-shifted (by 5.2 ppm relative to the GS) U38–N3 chemical shift strongly suggests a weakened hydrogen bond in ES2, either due to formation of a noncanonical base pair or a flipped-out bulge conformation (31) (Fig. 3*A*). The upfield-shifted base resonances for U25–C6 (1.5 ppm) and A35–C8 (2.4 ppm), which are bulged out in the GS, suggest increased stacking in ES2 (35), whereas the downfield-shifted base U23–C6 (2.3 ppm) suggests decreased stacking and possibly a flipped-out conformation (35) (Fig. 3*A*). The upfield-shifted A22–C1′ (2.2 ppm) and A27–C1′ (2.9 ppm) suggest sugar repuckering toward the C2′-endo conformation. Finally, the downfield-shifted G33–C1′ (2.4 ppm) and G33–C8 (2.5 ppm) strongly suggest a *syn* G33 base (36), and have chemical shifts very similar to the G(*syn*)–U transwobbles in closing base pairs of UNCG-type apical loops such as UUCG (37) and UGGG (16).

We previously showed (16) that secondary structure prediction programs such as MC-Fold (38) can help identify RNA ES as higher energy predicted secondary structures (16). MC-Fold correctly predicts the TAR GS and ES1 as the most (#1) and second-most (#2) energetically favorable secondary structures, respectively (Fig. 3*B*) (16). We therefore examined even higher energy structures predicted by MC-Fold that might account for the lower populated and energetically less favorable ES2. Structures #3 and #4 feature minor variations in the apical loop that cannot explain the apical loop ES2 chemical shifts or exchange at the bulge and upper stem (Fig. 3*B*). Although structure #5 may account for exchange at the bulge, it does not feature any changes in the apical loop and cannot explain why mutations in the apical loop quench exchange at the bulge (Fig. 2*B*). Strikingly, structures #6 and #7 (Fig. 3*B*) feature the desired simultaneous changes in the bulge, upper stem, and apical loop without affecting the lower stem, which shows little signs of exchange. This is accomplished by a global change in the register of bulge residues C24 and U25, which pair up with residues in the upper stem and result in reshuffling of base pairs that propagates to the apical loop through creation of three noncanonical base pairs (Fig. 3*B*). Structures #6 and #7 are predicted to have similar energetics and differ only with regard to whether U23 or nearby C24 forms a bulge. Whereas structure #7 better agrees with the structural features derived from chemical shifts particularly, we cannot rule out some degree of dynamic exchange between these two species in the ES.

Structure #7 explains the decreased stacking at U23 in ES2, which forms a single-nucleotide bulge, as well as sugar repuckering and backbone changes in the adjacent residue A22 toward the C2′-endo conformation (Fig. 3*B*). Structure #7 also features a U25–U38 noncanonical base pair which can perfectly explain the unusual upfield-shifted U38–N3 resonance (16) while also explaining increased stacking at U25 (Fig. 3*B*). The consecutive A27–G36 and G28–A35 mismatches (Fig. 3*B*) can account for increased stacking at A35 as well as C2′-endo sugar puckers for A27 and A35. Indeed, analysis of 13 G–A mismatches in the BioMagResBank database (39) shows that the majority (10 out of 13) of C1′ resonances of G–A mismatches are significantly

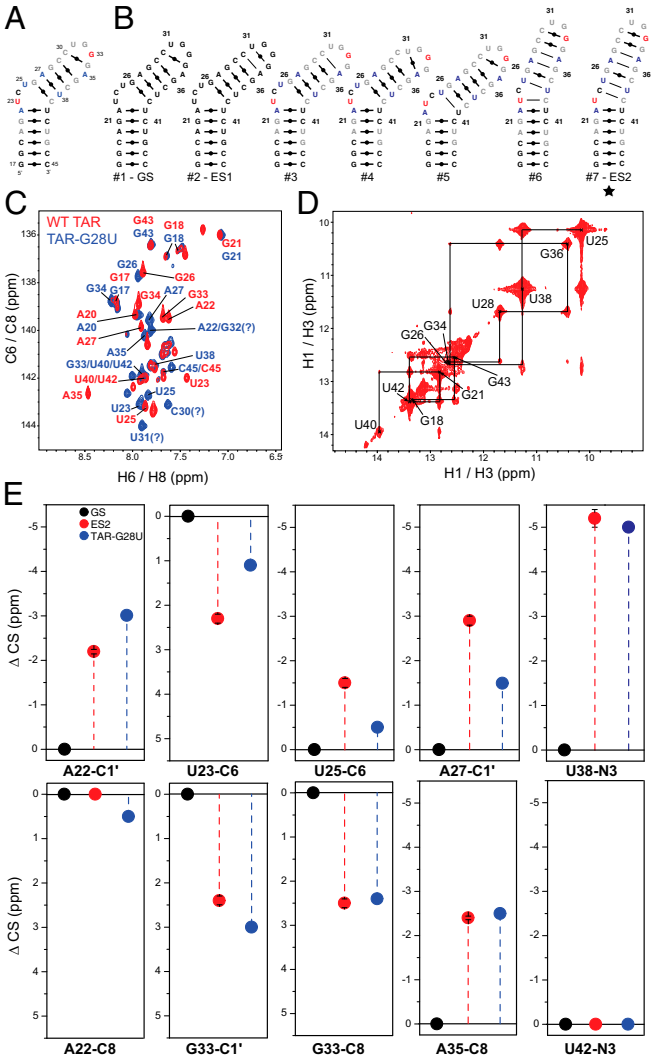

Fig. 3. Testing a candidate HIV-1 TAR ES structure using chemical shift fingerprinting. (*A*) GS secondary structure of HIV-1 TAR. Chemical shift fingerprints indicating increased stacking and/or *anti* glycosidic angles, loss of hydrogen bonds, and C2′-endo sugar pucker are in blue; decreased stacking and/or *syn* glycosidic angles, and C3′-endo sugar pucker are in red. Sites with little to no fast exchange are in gray. Sites at which the exchange could not be measured due to spectral overlap are in black. (*B*) HIV-1 TAR secondary structures predicted using MC-Fold (38). The residues of the structures from #3 to #7 are color-coded as described in *A*. The structure that best agrees with the R1ρ data is highlighted with a star. (*C*) Comparison of 2D C6/C8–H6/H8 heteronuclear single quantum coherence spectra of TAR-G28U and WT TAR. The assignments labeled with question marks are ambiguous. (*D*) Example imino proton NOE connectivity that supports the proposed secondary structure for TAR-G28U. (*E*) Chemical shift fingerprinting. Shown are the differences in chemical shifts determined using relaxation dispersion between the GS and GS (in red) and corresponding differences in chemical shifts obtained from comparing resonances in TAR-G28U (in blue) and the GS of WT TAR (in black). The error bars denote the SEs from the global fit.

upfield-shifted, consistent with C2′-endo sugar pucker. Importantly, structure #7 positions G33 at the apical loop closing base pair where it can form a G(*syn*)–C transwobble base pair, explaining the downfield-shifted G33–C8 and G33–C1′. Structure #7 also accounts for the absence of dispersion at the base moieties of G26, A27, G28, C29, G36, C37, and C39 given that these residues form base pairs in both the GS and ES2 (Fig. 1*A*). A transition toward structure #7 would minimally require the opening of a stable canonical A27–U38 base pair, consistent with

the measured activation free energy (16.8 kcal/mol; *SI Materials and Methods*, *Thermodynamic Analysis*), which is comparable to the energy needed to open RNA Watson–Crick base pairs (13–16 kcal/mol) (40). This can explain why the ES2 transition (k_{ex} ~ 474 Hz) is much slower than that observed for ES1 (k_{ex} ~ 25 kHz), which requires disruption of a weaker cross-stranded G34–C30 base pair.

Testing Candidate Structure for ES2 Using Mutate-and-Chemical-Shift Fingerprinting. We used a "Mutate-and-Chemical-Shift-Fingerprint" strategy (16) to test structure #7 as a candidate structure for ES2. In this approach, a mutation or chemical modification is introduced to trap a candidate ES structure. The chemical shifts of the trapped mutant are then compared with counterparts obtained for the ES using relaxation dispersion to determine whether the mutant is a good representation of the ES. We introduced a G28U point mutation targeting the center of the upper stem that is predicted by MC-Fold (38) to stabilize structure #7 through replacement of a noncanonical G28–A35 base pair with a more stable canonical U28–A35 base pair. This mutant was chosen among many options because it minimizes stabilization of other potentially competing low energy states while also avoiding changing residues that carry key chemical shift reporters.

The G28U point mutation resulted in large changes in chemical shifts throughout TAR and specifically at residues showing significant ES2 relaxation dispersion, including A22 in the lower stem, U23 and U25 in the bulge, A27 and U38 in the upper stem, and G33, G34, and A35 in the apical loop (Fig. 3*C* and Fig. S4*A*). These perturbations are consistent with a large change in secondary structure (Fig. 3*C*). As expected, the mutation caused minimal chemical shift perturbations at lower stem residues (G17, G18, A20, G21, U40, U42, G43, and C45; Fig. 3*C* and Fig. S4*A*), which show little to no signs of exchange in WT TAR.

Analysis of NMR spectra confirmed that TAR-G28U adopts the secondary structure predicted for structure #7. For example, we observed unique imino resonances and exchangeable–nonexchangeable NOE connectivities that establish formation of the G18–C44, C19–G43, A20–U42, G21–C41, A22–U40 base pairs in the lower stem and U25–U38, G26–C37, A27–G36, U28–A35, and C29–G34 base pairs in the upper stem (Fig. 3D and Fig. S4*B*). Although it was difficult to observe nonexchangeable NOE connectivity between G21 and A22 (Fig. S4*B*), possibly due to line broadening and exchange between structures #7 and #6 in TAR-G28U (Fig. 3*B*), we were able to trace these NOE connectivities using a second triple mutant (TAR-G28U/G36U/C39G) that is designed to trap structure #7 and destabilize structure #6, allowing for a complete sequential assignment of the lower stem (Fig. S5 *A* and *B*). In TAR-G28U, we observed a strong H8/H1′ NOE confirming that G33 adopts a *syn* base conformation along with a very strongly upfield-shifted G34–H1′ resonance (Fig. S4 *A* and *B*), which is characteristic of residues 3′-adjacent to *syn* G at tip of apical loops engaged in transwobble base pairs [e.g., G(*syn*)–U in cUUCGg tetraloop]. This is consistent with G33 forming a transwobble base pair with C30.

For all eight slow-exchanging resonances (A22–C1′, U23–C6, U25–C6, A27–C1′, G33–C8, G33–C1′, A35–C8, and U38–N3), we observe very good agreement between the differences in carbon and nitrogen chemical shifts when comparing spectra of TAR-G28U versus WT TAR and the corresponding differences in chemical shift between the ES2 and GS ($\Delta\omega$) measured by relaxation dispersion in WT TAR (Fig. 3*E*). The slightly poorer agreement (~1.5 ppm) observed for the magnitude (but not direction) of these shifts at A22–C1′, U23–C6, U25–C6, and A27–C1′ can be explained by proximity to the mutated site (A27–C1′), and possibly contributions from exchange with structure #6 in TAR-G28U (A22–C1′, U23–C6, and U25–C6). Although severely overlapped, the G33–C8 and G33–C1′ resonances in TAR-G28U assigned based on HCN through-bond correlation and NOESY experiments are downfield-shifted relative to WT TAR by 2.4 and 3.0 ppm, respectively, consistent with $\Delta\omega$ values of 2.5 and 2.4 ppm, respectively, measured by relaxation dispersion (Fig. 3*E*). Importantly, residues that show little or no sign of relaxation dispersion also have small differences in carbon or nitrogen chemical shifts (typically <0.5 ppm) between WT TAR and TAR-G28U, including G21–C1′, A22–C8, U23–C1′, A27–C2, G32–C1′, and U42–N3 (Fig. 3*E* and Fig. S6).

Reconciling ES1 and ES2 Relaxation Dispersion Contributions in the Apical Loop. Why do certain sites in the apical loop sense ES1 and not ES2, whereas other sites (16) sense ES2 and not ES1? Furthermore, why do certain sites not simultaneously sense ES1 and ES2 and therefore necessitate a three-state rather than two-state model to adequately explain the relaxation dispersion data? Some sites may not sense exchange to ES1 or ES2 because the accompanying change in chemical shift is small. Indeed, based on NMR spectra of an ES1 trapped TAR mutant (16), two of the three slow-exchanging apical loop resonances (G33–C1′ and G33–C8) are not expected to sense ES1 because the difference in chemical shift is <0.5 ppm. For the third slowly exchanging resonance, A35–C8, it is not possible to independently assess the difference in chemical shifts between GS and ES1 because this is the site of mutation (16). Likewise, among five fast-exchanging resonances, A35–C1′ and G34–C8 are not expected to sense ES2 because the difference in chemical shifts between the GS and ES2 is <0.5 ppm based on the comparison of spectra of WT TAR and the ES2 trapped mutant (Fig. 3*C* and Fig. S4*A*).

In contrast, however, the fast-exchanging resonances C30–C1′, U31–C1′, and G34–C1′ are expected to experience a sizable change in chemical shift due to exchange with ES2 (Fig. S4*A*). Attempts to fit these fast-exchanging resonances to a three-state model (41) (ES1 ←→ GS ←→ ES2) did not yield robust fitting and resulted in very high uncertainties in the derived exchange parameters. This is not surprising given that the relaxation contribution due to chemical exchange (R_{ex}) with the highly populated ES1 (R_{ex} ~ 16–21 Hz) is twofold to fivefold greater than corresponding R_{ex} with ES2 (R_{ex} ~ 3–10 Hz). As a result, R_{ex} contributions due to ES2 may be masked by the larger contributions from ES1, such that it becomes difficult to measure within experimental uncertainty in a three-state fit.

To resolve slow exchange to ES2 in the apical loop resonances C30–C1′, U31–C1′, and G34–C1′ that may be masked by fast

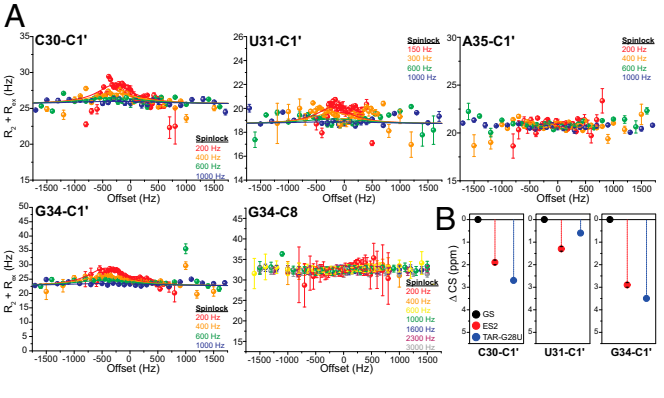

Fig. 4. Separating ES1 and ES2 contributions to R1ρ relaxation dispersion by increasing temperature to 35 °C. (*A*) Off-resonance profiles of C30–C1′, U31–C1′, A35–C1′, G34–C1′, and G34–C8. Shown are global fits (solid line) to a two-state Laguerre exchange model (Eq. **S1**). Error bars represent experimental uncertainty (1 SD) as determined from propagation of errors obtained from monoexponential fitting of duplicate sets of R1ρ data and analysis of signal-to-noise. (*B*) Chemical shift fingerprinting of nuclei showing dispersion at 35 °C. The color scheme follows that of Fig. 3*E*. The error bars denote the SEs from the global fit.

exchange, we carried out relaxation dispersion experiments at a higher temperature of 35 °C, with the goal of pushing the fast ES1 process outside the detection limit of R1ρ relaxation dispersion (42). Indeed, increasing the temperature to 35 °C quenched the relaxation dispersion in fast-exchanging G34–C8 and A35–C1′ resonances, which are not expected to sense ES2 ($\Delta\omega \sim 0$ ppm) (Fig. 4*A*), indicating that the fast process falls outside the limit of R1ρ detection at 35 °C. Conversely, increasing the temperature to 35 °C had little effect on slow-exchanging apical loop resonances (Fig. S7 and Table S1). A two-state analysis of these relaxation dispersion data (Table S1) yielded populations (p_B = ~0.2%) and chemical shifts very similar to those measured for ES2 at 25 °C with the expected slightly higher exchange rates (k_{ex} = ~2,100 Hz compared with ~474 Hz at 25 °C).

Interestingly, fast-exchanging apical loop resonances C30–C1′, U31–C1′, and G34–C1′, which are expected to sense ES2, start to exhibit slow exchange (k_{ex} = 1,552–2,666 Hz) at 35 °C (Fig. 4*A*). A two-state analysis of these relaxation dispersion data yields an ES with $p_B \sim 0.2\%$ and lifetime ~0.47 ms that is in very good agreement with ES2 parameters deduced from slow-exchanging resonances at the same temperature (Table S1). Moreover, the ES chemical shifts for this slower process that emerges at 35 °C are in very good agreement with those obtained for the TAR-G28U ES2 trapped mutant (Fig. 4*B*). For example, G34–C1′ is 2.9 ppm downfield-shifted relative to the GS, which is in good agreement with the ~3.5-ppm downfield shift observed when comparing spectra of WT TAR and TAR-G28U at 35 °C. This downfield shift is also consistent with G34–C1′ being adjacent to G33(*syn*)–C30 transwobble base pair in ES2 (Fig. 3*B*). Although we were not able to unambiguously assign C30–C1′ and U31–C1′ in TAR-G28U due to severe spectral overlap, they could tentatively be assigned based on HCN experiments and comparison with spectra of TAR-UUCG (43), which has a similar tetraloop. The ES2 chemical shifts for both C30–C1′ and U31–C1′ obtained from relaxation dispersion data measured at 35 °C are downfield-shifted by 1.9 and 1.3 ppm, respectively, in good agreement with downfield shifts of 2.7 and 0.6 ppm, respectively, obtained by comparing spectra of WT TAR and TAR-G28U (Fig. 4*B*).

We were able to fit the relaxation dispersion data measured for C30–C1′, U31–C1′, and G34–C1′ at 25 °C (16) to a star-like three-state exchange model (ES1 ←→ GS ←→ ES2) when fixing ES2 exchange parameters (k_{ex} and p_B) to those obtained from a two-state global fit of the eight slow-exchanging resonances (Table S1) and assuming the $\Delta\omega$-values obtained from relaxation dispersion data measured at 35 °C. The fit was of equal or better quality for the three-state compared with two-state exchange model, as assessed using the Akaike Information Criterion test (Table S2). Thus, all relaxation dispersion data measured in TAR can be accommodated within a framework that includes exchange between GS, ES1, and ES2 (Fig. 5).

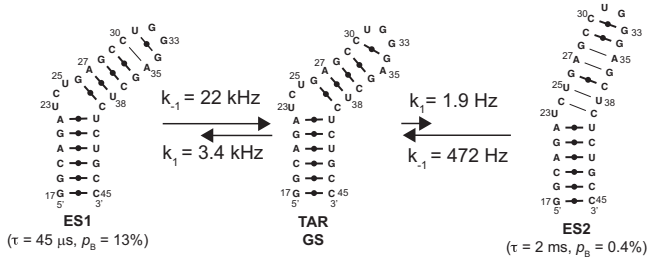

Fig. 5. Proposed three-state exchange in HIV-1 TAR. Shown are the secondary structures of ES1 and ES2 along with their population (p_B) and lifetime (τ), as well as forward (k_1) and backward (k_{-1}) rate constants.

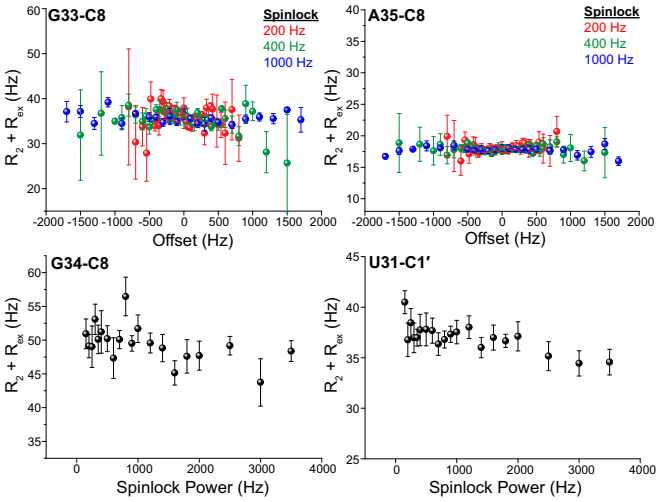

Fig. 6. Quenching of slow and fast R1ρ relaxation dispersion at the apical loop through binding of the ligand ARG. Shown are off-resonance relaxation dispersion profiles for ES2 resonances (G33–C8 and A35–C8) and the on-resonance relaxation dispersion profiles for ES1 resonances (G34–C8 and U31–C1′). Error bars represent experimental uncertainty (1 SD) as determined from propagation of errors obtained from monoexponential fitting of duplicate sets of R1ρ data and analysis of signal-to-noise.

Impact of Argininamide Binding. Correlated exchange at the apical loop and bulge provides a basis for long-range communication in HIV-1 TAR. To test this possibility, we examined whether binding of argininamide (ARG), a ligand mimic of TAR's cognate protein target Tat, to the TAR bulge affects relaxation dispersion measured in the apical loop. Previous NMR studies (25, 44) showed that ARG binds TAR in and around the bulge stabilizing a coaxial conformation in which bulge residue U23 forms a reverse Hoogsteen base pair with A27–U38 in the upper stem. If our proposed ES2 structure is correct, one would expect that locking the bulge conformation upon ARG binding would quench all relaxation dispersion arising due to exchange with ES2, including in the apical loop. Indeed, addition of ARG (11 mM) to TAR (0.7 mM) quenched the relaxation dispersion at the slow-exchanging sites in the apical loop (G33–C8 and A35–C8, Fig. 6). Interestingly, ARG binding also quenched relaxation dispersion at fast-exchanging sites (U31–C1′ and G34–C8) (Fig. 6). This could be due to secondary binding to the apical loop (45, 46) especially given the high concentration of ARG used in our study. Thus, although we observe the expected quenching of relaxation dispersion at slow-exchanging sites in the apical loop, we cannot rule out that this arises due to direct binding of ARG to the apical loop.

Conclusion

We have characterized an ES structure for HIV-1 TAR that simultaneously remodels the bulge, upper stem, and apical loop. This ES reveals a mechanism for dynamically coupling distant RNA motifs; the TAR bulge and apical loop are separated by four canonical Watson–Crick base pairs, yet mutations that target either the bulge or apical loop have profound effects on exchange with ES2. Such long-range communication may provide a mechanism for achieving cooperativity during RNA folding and RNP assembly (47). Indeed, there is evidence for coupling between the TAR bulge and apical loop, including data showing that the proteins Tat and cyclin T1, which interact with the TAR bulge and apical loop, respectively, bind to TAR cooperatively (48). This ES structure may be involved in the many distinct functions attributed to TAR, and possibly play roles mediating interactions with many

viral and host proteins that are thought to bind TAR (27, 28). The TAR ES also represents a target for developing anti-HIV therapeutics given that the structure is unlikely to support Tat-mediated transactivation. Together with the previously characterized ES1, which has populations and lifetimes that differ by orders of magnitude compared with ES2, our study reveals yet another layer of rich complexity in the RNA dynamic structure landscape that may be harnessed to execute unique functions.

Materials and Methods

RNA samples for NMR were prepared by in vitro transcription as described in *SI Materials and Methods*. All NMR relaxation dispersion experiments were performed on a Bruker Avance 600-MHz NMR spectrometer equipped with a 5-mm cryogenic probe. Details on the NMR experiments and data analysis are described in *SI Materials and Methods*.

ACKNOWLEDGMENTS. We thank Zachary W. Stein and Mitchell McBrairty for input and assistance. This work was supported by the US National Institutes of Health (R01 AI066975).

1. Dethoff EA, Chugh J, Mustoe AM, Al-Hashimi HM (2012) Functional complexity and regulation through RNA dynamics. *Nature* 482(7385):322–330.
2. Leulliot N, Varani G (2001) Current topics in RNA-protein recognition: Control of specificity and biological function through induced fit and conformational capture. *Biochemistry* 40(27):7947–7956.
3. Hoogstraten CG, Sumita M (2007) Structure-function relationships in RNA and RNP enzymes: Recent advances. *Biopolymers* 87(5-6):317–328.
4. Kim JN, Breaker RR (2008) Purine sensing by riboswitches. *Biol Cell* 100(1):1–11.
5. Grundy FJ, Winkler WC, Henkin TM (2002) tRNA-mediated transcription antitermination in vitro: Codon-anticodon pairing independent of the ribosome. *Proc Natl Acad Sci USA* 99(17):11121–11126.
6. Mulder AM, et al. (2010) Visualizing ribosome biogenesis: Parallel assembly pathways for the 30S subunit. *Science* 330(6004):673–677.
7. Schwalbe H, Buck J, Fürtig B, Noeske J, Wöhnert J (2007) Structures of RNA switches: Insight into molecular recognition and tertiary structure. *Angew Chem Int Ed Engl* 46(8):1212–1219.
8. Lu K, Heng X, Summers MF (2011) Structural determinants and mechanism of HIV-1 genome packaging. *J Mol Biol* 410(4):609–633.
9. Herschlag D, Khosla M, Tsuchihashi Z, Karpel RL (1994) An RNA chaperone activity of non-specific RNA binding proteins in hammerhead ribozyme catalysis. *EMBO J* 13(12): 2913–2924.
10. Yang Q, Jankowsky E (2005) ATP- and ADP-dependent modulation of RNA unwinding and strand annealing activities by the DEAD-box protein DED1. *Biochemistry* 44(41): 13591–13601.
11. Wickiser JK, Winkler WC, Breaker RR, Crothers DM (2005) The speed of RNA transcription and metabolite binding kinetics operate an FMN riboswitch. *Mol Cell* 18(1): 49–60.
12. Sekhar A, Kay LE (2013) NMR paves the way for atomic level descriptions of sparsely populated, transiently formed biomolecular conformers. *Proc Natl Acad Sci USA* 110(32):12867–12874.
13. Palmer AG, 3rd (2014) Chemical exchange in biomacromolecules: Past, present, and future. *J Magn Reson* 241(0):3–17.
14. Hoogstraten CG, Wank JR, Pardi A (2000) Active site dynamics in the lead-dependent ribozyme. *Biochemistry* 39(32):9951–9958.
15. Blad H, Reiter NJ, Abildgaard F, Markley JL, Butcher SE (2005) Dynamics and metal ion binding in the U6 RNA intramolecular stem-loop as analyzed by NMR. *J Mol Biol* 353(3):540–555.
16. Dethoff EA, Petzold K, Chugh J, Casiano-Negroni A, Al-Hashimi HM (2012) Visualizing transient low-populated structures of RNA. *Nature* 491(7426):724–728.
17. Hansen AL, Nikolova EN, Casiano-Negroni A, Al-Hashimi HM (2009) Extending the range of microsecond-to-millisecond chemical exchange detected in labeled and unlabeled nucleic acids by selective carbon R(1rho) NMR spectroscopy. *J Am Chem Soc* 131(11):3818–3819.
18. Massi F, Johnson E, Wang C, Rance M, Palmer AG, 3rd (2004) NMR R1 rho rotating-frame relaxation with weak radio frequency fields. *J Am Chem Soc* 126(7):2247–2256.
19. Korzhnev DM, Orekhov VY, Kay LE (2005) Off-resonance R(1rho) NMR studies of exchange dynamics in proteins with low spin-lock fields: An application to a Fyn SH3 domain. *J Am Chem Soc* 127(2):713–721.
20. Bannwarth S, Gatignol A (2005) HIV-1 TAR RNA: The target of molecular interactions between the virus and its host. *Curr HIV Res* 3(1):61–71.
21. Bieniasz PD, Grdina TA, Bogerd HP, Cullen BR (1999) Recruitment of cyclin T1/P-TEFb to an HIV type 1 long terminal repeat promoter proximal RNA target is both necessary and sufficient for full activation of transcription. *Proc Natl Acad Sci USA* 96(14): 7791–7796.
22. Benkirane M, et al. (1997) Oncogenic potential of TAR RNA binding protein TRBP and its regulatory interaction with RNA-dependent protein kinase PKR. *EMBO J* 16(3): 611–624.
23. Das AT, Vrolijk MM, Harwig A, Berkhout B (2012) Opening of the TAR hairpin in the HIV-1 genome causes aberrant RNA dimerization and packaging. *Retrovirology* 9(1):59.
24. Klase Z, et al. (2007) HIV-1 TAR element is processed by Dicer to yield a viral micro-RNA involved in chromatin remodeling of the viral LTR. *BMC Mol Biol* 8(1):63.
25. Puglisi JD, Tan R, Calnan BJ, Frankel AD, Williamson JR (1992) Conformation of the TAR RNA-arginine complex by NMR spectroscopy. *Science* 257(5066):76–80.
26. Aboul-ela F, Karn J, Varani G (1996) Structure of HIV-1 TAR RNA in the absence of ligands reveals a novel conformation of the trinucleotide bulge. *Nucleic Acids Res* 24(20):3974–3981.
27. Kim I, Liu CW, Puglisi JD (2006) Specific recognition of HIV TAR RNA by the dsRNA binding domains (dsRBD1-dsRBD2) of PKR. *J Mol Biol* 358(2):430–442.
28. Gatignol A, Buckler-White A, Berkhout B, Jeang K-T (1991) Characterization of a human TAR RNA-binding protein that activates the HIV-1 LTR. *Science* 251(5001): 1597–1600.
29. Davidson A, et al. (2009) Simultaneous recognition of HIV-1 TAR RNA bulge and loop sequences by cyclic peptide mimics of Tat protein. *Proc Natl Acad Sci USA* 106(29): 11931–11936.
30. Stelzer AC, et al. (2011) Discovery of selective bioactive small molecules by targeting an RNA dynamic ensemble. *Nat Chem Biol* 7(8):553–559.
31. Nikolova EN, Gottardo FL, Al-Hashimi HM (2012) Probing transient Hoogsteen hydrogen bonds in canonical duplex DNA using NMR relaxation dispersion and single-atom substitution. *J Am Chem Soc* 134(8):3667–3670.
32. Miloushev VZ, Palmer AG, 3rd (2005) R(1rho) relaxation for two-site chemical exchange: General approximations and some exact solutions. *J Magn Reson* 177(2): 221–227.
33. Dethoff EA, et al. (2008) Characterizing complex dynamics in the transactivation response element apical loop and motional correlations with the bulge by NMR, molecular dynamics, and mutagenesis. *Biophys J* 95(8):3906–3915.
34. Wunderlich CH, et al. (2012) Synthesis of (6-(13)C)pyrimidine nucleotides as spin-labels for RNA dynamics. *J Am Chem Soc* 134(17):7558–7569.
35. Xu X-P, Au-Yeung SCF (2000) Investigation of chemical shift and structure relationships in nucleic acids using NMR and density functional theory methods. *J Phys Chem B* 104(23):5641–5650.
36. Ghose R, Marino JP, Wiberg KB, Prestegard JH (1994) Dependence of 13C chemical shifts on glycosidic torsional angles in ribonucleic acids. *J Am Chem Soc* 116(19): 8827–8828.
37. Nozinovic S, Fürtig B, Jonker HR, Richter C, Schwalbe H (2010) High-resolution NMR structure of an RNA model system: The 14-mer cUUCGg tetraloop hairpin RNA. *Nucleic Acids Res* 38(2):683–694.
38. Parisien M, Major F (2008) The MC-Fold and MC-Sym pipeline infers RNA structure from sequence data. *Nature* 452(7183):51–55.
39. Ulrich EL, et al. (2008) BioMagResBank. *Nucleic Acids Res* 36(Database issue, suppl 1): D402–D408.
40. Snoussi K, Leroy JL (2001) Imino proton exchange and base-pair kinetics in RNA duplexes. *Biochemistry* 40(30):8898–8904.
41. Trott O, Palmer AG, 3rd (2004) Theoretical study of R(1rho) rotating-frame and R2 free-precession relaxation in the presence of n-site chemical exchange. *J Magn Reson* 170(1):104–112.
42. Bothe JR, Stein ZW, Al-Hashimi HM (2014) Evaluating the uncertainty in exchange parameters determined from off-resonance R1ρ relaxation dispersion for systems in fast exchange. *J Magn Reson* 244C:18–29.
43. Zhang Q, Sun X, Watt ED, Al-Hashimi HM (2006) Resolving the motional modes that code for RNA adaptation. *Science* 311(5761):653–656.
44. Pitt SW, Majumdar A, Serganov A, Patel DJ, Al-Hashimi HM (2004) Argininamide binding arrests global motions in HIV-1 TAR RNA: Comparison with Mg2+-induced conformational stabilization. *J Mol Biol* 338(1):7–16.
45. Bardaro MF, Jr., Shajani Z, Patora-Komisarska K, Robinson JA, Varani G (2009) How binding of small molecule and peptide ligands to HIV-1 TAR alters the RNA motional landscape. *Nucleic Acids Res* 37(5):1529–1540.
46. Davis B, et al. (2004) Rational design of inhibitors of HIV-1 TAR RNA through the stabilisation of electrostatic "hot spots.". *J Mol Biol* 336(2):343–356.
47. Williamson JR (2008) Cooperativity in macromolecular assembly. *Nat Chem Biol* 4(8): 458–465.
48. Wei P, Garber ME, Fang S-M, Fischer WH, Jones KA (1998) A novel CDK9-associated C-type cyclin interacts directly with HIV-1 Tat and mediates its high-affinity, loop-specific binding to TAR RNA. *Cell* 92(4):451–462.